Tellus (1999), 51A-B, 91–109
Printed in UK – all rights reserved

TELLUS
ISSN 0280–6495
ISSN 0280–6509

The rôle of thermohaline circulation in climate

By SYUKURO MANABE[1]* and RONALD J. STOUFFER[2], [1]*Institute for Global Change Research, Frontier Research System for Global Change, 7F SEAVANS-N Bldg., Shibaura 1-2-1, Minato-ku, Tokyo 105-6791, Japan and* [2]*Geophysical Fluid Dynamics Laboratory/NOAA, Princeton University, Princeton, New Jersey 08542, USA*

(Manuscript received 10 June 1998; in final form 22 September 1998)

ABSTRACT

This article discusses the rôle of the THC in climate, based upon the results of several numerical experiments which use a coupled ocean-atmosphere model developed at the Geophysical Fluid Dynamics Laboratory of NOAA, USA. The first part of the article explores the mechanism which is responsible for the abrupt climate change such as the Younger Dryas event using the coupled model. In response to the freshwater discharge into high north Atlantic latitudes over a period of 500 years, the THC in the Atlantic Ocean weakens, reducing surface air temperature over the northern north Atlantic Ocean, the Scandinavian Peninsula, and the circumpolar ocean and Antarctic Continent of the southern hemisphere. Upon the termination of the water discharge at the 500th year, the THC begins to intensify, regaining its original intensity in a few hundred years. In addition, the sudden onset and the termination of the discharge of freshwater induces the multidecadal fluctuation in the intensity of the THC, which generates the almost abrupt change of climate. It is noted that similar but much weaker oscillation of the THC is also evident in the control integration of the coupled model without freshwater forcing. The irregular oscillation of the THC mentioned above appears to be related to the fluctuation of the Subarctic Gyre and associated east Greenland current, yielding the evolution of the surface salinity anomaly which resembles that of "great salinity anomaly". The second part of this article describes the response of a coupled ocean-atmosphere model to the doubling and quadrupling of atmospheric carbon dioxide over centuries time-scale. In one integration, the CO_2 concentration increases by 1%/year (compounded) until it reaches 4× the initial value at the 140th year and remains unchanged thereafter. In another integration, the CO_2 concentration also incleases at the rate of 1%/year until it reaches 2× the initial value at the 70th year and remains unchanged thereafter. One of the most notable features of the CO_2-quadrupling integration is the gradual disappearance of thermohaline circulation in most of the model oceans during the first 250-year period, leaving behind wind-driven cells. For example, thermohaline circulation nearly vanishes in the north Atlantic by the 250 years of the integration and remains very weak until the 900th year. However, it begins to restore the original intensity by the 1600th year. In the CO_2-doubling integration, the thermohaline circulation weakens by a factor of more than 2 in the North Atlantic during the first 150 years, but almost recovers its original intensity by the 500th year. The weakening of the THC moderates temporarily the greenhouse warming over the north Atlantic Ocean and its vicinity. In both numerical experiments described above, the initial weakening of the THC results from the capping of oceanic surface by relatively fresh, low-density water, which surpresses the convective cooling of water in the sinking region of the THC.

1. Introduction

One of the most valuable tools used for the study of climate is a coupled ocean-atmosphere model in which general circulation models of the atmosphere and ocean are combined with that of oceans. It was the late 1960s when Manabe and Bryan (1969) developed and used a coupled ocean-atmosphere model in order to explore the rôle of oceanic circulation in maintaining climate. This paper explores the rôle of the thermohaline circu-

* Corresponding author.
email: sm@frontier.esto.or.jp

lation in shaping climatic change, based upon the results from recent studies which use a coupled ocean-atmosphere model developed at the Geophysical Fluid Dynamics Laboratory of NOAA.

In the Atlantic Ocean, the THC transports warm saline surface water towards high latitudes, thereby keeping the sea-surface temperature of the northern North Atlantic higher than that of the northern North Pacific at comparable latitudes. Thus, the change in the intensity of the THC could alter the distribution of surface temperature in the North Atlantic Ocean and surrounding regions. Examples of such phenomena include the so-called abrupt climate changes associated with the Younger Dryas event which occurred during the last deglacial periods. Broecker et al. (1985) speculated that these abrupt climate changes result from the abrupt shift of the THC from one mode of operation to another. The first half of this paper discusses our attempt to explore these abrupt climate changes using a coupled ocean-atmosphere model (Manabe and Stouffer, 1988, 1995, 1997). Based upon the results from the study of Manabe and Stouffer (1993, 1994), the second half of this study explores the rôle of the THC in shaping the change of a simulated climate which occurs in response to gradual increase in the atmospheric concentration of carbon dioxide.

2. Coupled model

2.1. Model structure

The coupled atmosphere-ocean-land surface model used here was developed to study the climate response to increasing greenhouse gases, and will hereafter be called the coupled model, for simplicity. The structure and performance of the model were described by Manabe et al. (1991), hereafter identified as M91. Therefore, only a brief description of the model structure is given here.

The coupled model (Fig. 1) consists of general circulation models (GCM) of the atmosphere and ocean, and a simple model of the continental surface that involves the budgets of heat and water (Manabe, 1969). It is a global model with realistic geography limited by its resolution. It has 9 vertical finite difference levels. The horizontal distributions of predicted variables are represented by spherical harmonics (15 associated Légendre functions for each of 15 Fourier components) and by gridpoint values (Gordon and Stern, 1982). The model has a simple parameterization of land-surface process to compute surface fluxes of heat and water. Insolation varies seasonally, but not diurnally. The model predicts cloud cover which depends only on relative humidity.

The ocean GCM (Bryan and Lewis, 1979) uses

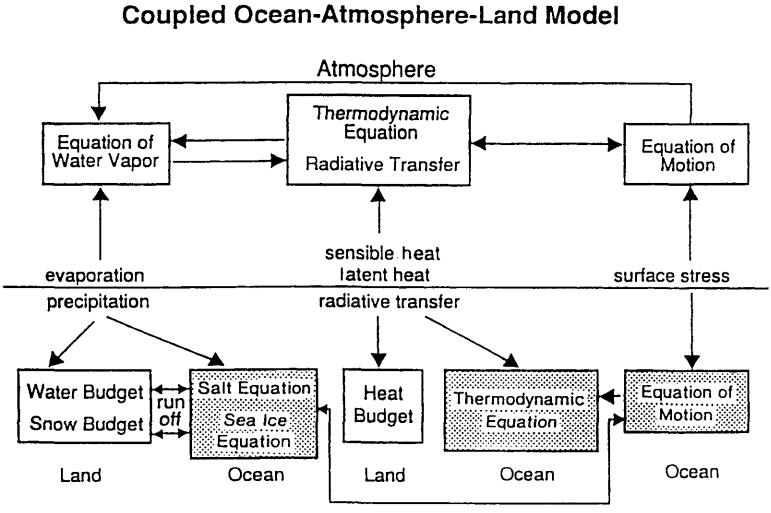

Fig. 1. The structure of the coupled ocean-atmosphere model.

a full finite-difference technique and has a regular grid system with approximately 4° latitude by 3.7° longitude spacing. There are 12 vertical finite-difference levels. The atmospheric and oceanic components of the model interact with each other once each day through the exchange of heat, water, and momentum fluxes. A simple sea ice model is also incorporated into the coupled model. It predicts sea ice thickness, based upon thermodynamic heat balance and incorporating the effect of ice advection by ocean currents. For further details of the coupled model, see M91. Dixon et al. (1996) also describe the ability of the model to simulate the uptake of anthropogenic trichlorofluromethane (CFC-11) by the ocean.

2.2. *Time integration*

Initial conditions for the time integration of the coupled model include realistic seasonal and geographical distributions of surface temperature, surface salinity, and sea ice of the present, with which both the atmospheric and oceanic model states are nearly in equilibrium. When the time integration of the model starts from this initial condition, the model climate drifts toward its own equilibrium state, which differs from the initial condition described above. To reduce this drift, the fluxes of heat and water imposed at the oceanic surface (including sea ice-covered areas) of the coupled model are modified by amounts that vary geographically and seasonally but do not change from one year to the next (for details, see M91 and Manabe and Stouffer, 1994)). Since the adjustments are determined prior to the time integration of the coupled model and are not correlated with the transient anomalies of SST (i.e., sea-surface temperature) and SSS (i.e., sea-surface salinity), which can develop during the integration, they are unlikely to either systematically amplify or dampen the anomalies. Owing to the flux adjustment technique, the model fluctuates around a realistic equilibrium state.

Starting from the initial condition that was obtained and described above, the coupled model is integrated over a period of 1000 years. Owing to the application of the flux adjustments, the mean trend in global mean surface air temperature during this period is only -0.023C century^{-1}. The trend of global mean temperature in the deeper layers of the model ocean is somewhat larger at -0.07C century^{-1}. This trend appears to result from the imperfection of the procedures used for determining the initial condition and time integration of the coupled model. The specific reasons for this trend, however, have not been identified and are under investigation.

3. Abrupt climate changes

3.1. *Younger Dryas event*

Isotopic analysis of Greenland ice cores suggests that large and rapid changes of climate occurred frequently during the last glacial and deglacial periods. For example, the isotopic (δ_{18}O) temperature dropped very rapidly approximately 13 000 years ago, followed by the so-called Younger Dryas event (Y-D) when the isotopic temperature was almost as low as at the last glacial maximum. Faunal and palynological analyses indicate that during the cold Y-D period, surface temperatures were very low not only over the northern North Atlantic but also over western Europe. The Y-D period lasted several hundred years and ended abruptly, as indicated by the records from Greenland ice cores. As noted in Section 1, Broecker et al. (1985) suggested that such an abrupt change resulted from a very rapid change in the thermohaline circulation (THC). They further speculated that meltwater from continental ice sheets caused the capping of the oceanic surface by relatively freshwater in high North Atlantic latitudes and was responsible for the rapid weakening of THC and the abrupt cooling of climate.

This paper explores the physical mechanism of abrupt climate change based mainly upon the results from a set of numerical experiments conducted at the Geophysical Fluid Dynamics Laboratory of NOAA (Manabe and Stouffer, 1997 identified hereafter as MS97). Particularly, it attempts to elucidate the rôle of the thermohaline circulation (THC) in inducing the abrupt climate change; see MS97 for further discussion of the locations of freshwater discharge and its impact on the THC during the Bölling/Alleröd Y-D period.

3.2. *Freshwater experiment*

The simulated modern state of the coupled ocean-atmosphere system, which is obtained from the time integration described in Subsection 2.2 is used as the control for the freshwater experiments conducted in the present study. Instead, one could have used as a control a coupled model state of the last deglaciation period when a major fraction of the continental ice sheets of the last glacial period still remained. Since the response of the cold, glacial state of the coupled ocean-atmosphere system to freshwater discharge could be different from the corresponding response of the interglacial, modern state (Winton, 1997), it is highly desirable to conduct the numerical experiments using boundary conditions of the last deglaciation period. Unfortunately, we have not succeeded in simulating either the glacial or deglacial world using a coupled ocean-atmosphere GCM. Therefore, we used the simulated modern state of the coupled model as a control and perturbed it with an input of freshwater into the North Atlantic Ocean.

In addition to the control integration described in Subsection 2.2, two numerical integrations are conducted for the present study. The initial condition for both integrations is the state of the coupled model at the 500th year of the control integration. In Subsection 3.3, we discuss the results from one of these two integrations in which freshwater is discharged at the rate of 0.1 Sv (one sverdrup = 10^6 m^3 s^{-1}) uniformly over the 50°N–70°N belt of the North Atlantic Ocean (identified as domain A in Fig. 2) over the period of 500 years. After the termination of the freshwater discharge, the time integration is continued for the additional 750 years until the 1250th year. By comparing this "freshwater integration" with the control over the corresponding period of 1250 years, the impact of freshwater input upon the coupled ocean-atmosphere system is investigated.

3.3. *Model response*

In response to the sustained, massive freshwater discharge described above, the region of low sea-surface salinity (SSS) spreads down to 30°N–40°N (Fig. 3), creating an intense halocline several hundred meters beneath the surface. The surface layer of relatively fresh, low-density water prevents the

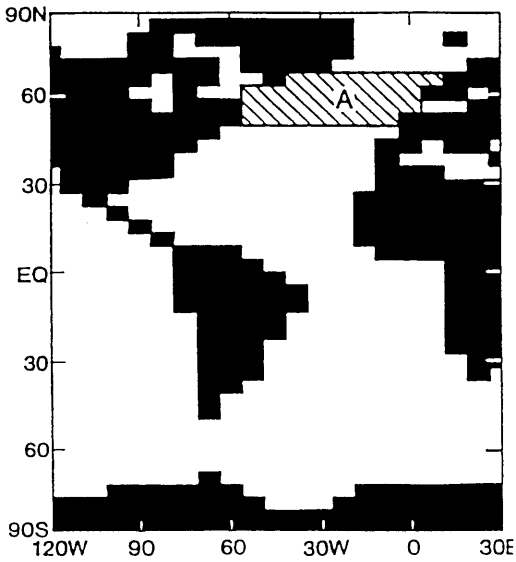

Fig. 2. Region A indicates the area where freshwater is discharged in the freshwater integration (from MS97).

convective cooling of the water column and the production of negative buoyancy in the sinking region of the thermohaline circulation (THC) in the northern North Atlantic, thereby weakening the THC throughout the 500-year period of the freshwater discharge. The streamfunction of the meridional overturning in the Atlantic Ocean (Fig. 4) indicates that the THC not only weakens but also becomes much shallower (Fig. 4b). Meanwhile, the northward flow of Antarctic bottom water extends northward, thereby intensifying the reverse overturning cell near the bottom of the Atlantic Ocean (Fig. 4b). Following the termination of freshwater discharge on the 500th year, the THC reintensifies and fully recovers its original intensity and distribution by the 900th year (Fig. 4c).

As the intensity of the THC weakens, the surface currents in the North Atlantic Ocean also undergo marked changes, which can be inferred by comparing Figs. 5a, and b, e.g., the North Atlantic current, which extends from the coast of the Southeast US towards the Norwegian Sea, also weakens in the Atlantic during the period of the freshwater discharge. Thus, the warm, saline surface water in the subtropical Atlantic hardly penetrates into the northern North Atlantic Ocean towards the end of the 500-year period of freshwater discharge. On

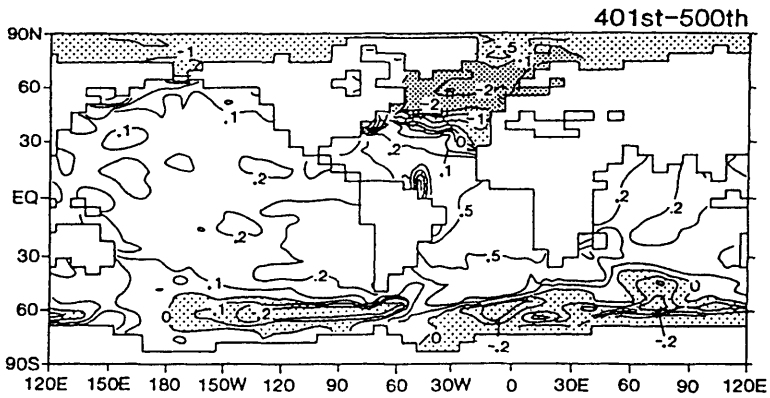

Fig. 3. The geographical distribution of SSS anomalies (psu) averaged over years 401–500. The anomalies represent the difference between the freshwater and the control integrations. Contours are in logarithmic intervals for values of 0, ± 0.1, ± 0.2, ± 0.5, ± 1 and ± 2 (from MS97).

the other hand, the Subarctic Gyre and associated east Greenland current become more intense and extend southwards (Fig. 5b). It is of particular interest that the intensified Labrador current and its southeastward extension in the model results track the path of ice-rafted debris during the so-called Heinrich events (Bond et al., 1992), which often occurred during cold periods of Dansgaad-Oeschger oscillation.

Associated with the weakening of the THC described above, the northward advection of the warm and saline surface water is reduced, causing a large reduction in sea-surface temperature (SST) in the northern North Atlantic (Fig. 6). The local maximum in cooling located south of Greenland, however, is attributable to the intensification and the southward extension of the east Greenland current (Fig. 5) which advects cold Arctic surface water southward.

Interestingly, an extensive region of SST reduction appears not only in the North Atlantic but also in the circumpolar ocean of the Southern Hemisphere. The cold anomaly in the Pacific sector continues to intensify until the 800th year of the integration. Preliminary analysis (MS97) indicates that this anomaly results from the delayed weakening of the deep reverse THC cell involving the Antarctic bottom water in the Pacific Ocean. The weakening increases the meridional SST gradient of the circumpolar ocean and intensifies the surface westerlies which, in turn, reduces SST by enhancing the northward Ekman drift of cold surface water and sea ice and further increases the meridional SST gradient. For further detail of the results of this analysis, refer to MS97.

The freshwater-induced change of sea-surface temperature described above affects the overlying atmosphere, causing a reduction in surface air temperature over an extensive region (Fig. 7). The cooling is particularly large over the northern North Atlantic and the Nordic Seas, and extends over not only Greenland but also the Arctic Ocean, the Scandinavian Peninsula, and western Europe (Fig. 7). Furthermore, small negative anomalies extend over most of the high northern latitudes. The cooling centered around Iceland increases until the end of the freshwater discharge (i.e., the 500th year of the experiment), but decreases rapidly thereafter and disappears completely by the 750th year. Negative anomalies also appear in the Indian and Pacific sectors of the circumpolar ocean of the southern hemisphere, extending to the Antarctic Continent. On the other hand, very small positive SST anomalies cover the rest of the world. The global mean change of surface air temperature are small throughout the course of the experiment, because small but extensive positive temperature anomalies compensate for the large but geographically limited negative anomalies.

The distribution of the freshwater-induced change in surface air temperature described above is consistent with the map of the surface temperature difference between the Y-D and Alleröd, which was prepared by D. Peteet (Broecker, 1995) based upon the analysis of oceanic and bog sedi-

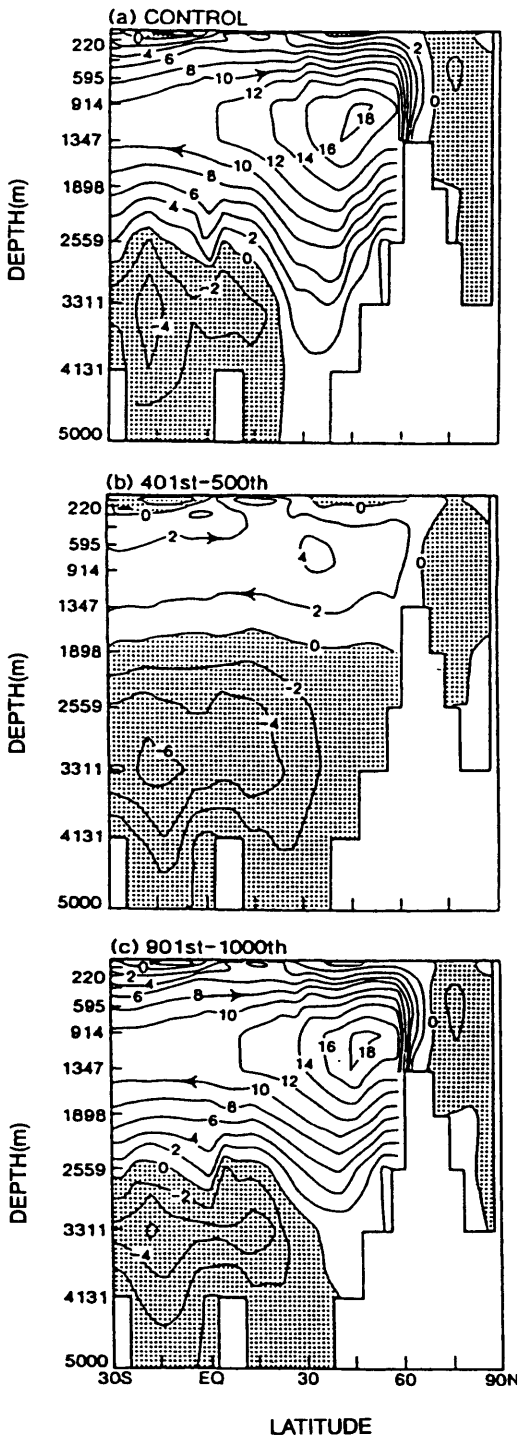

ments (Fig. 8). Over the western Europe and Labrador Peninsula, for example, palynological records indicate the Y-D cooling of significant magnitude, whereas they do not over most of the North American Continent. The qualitative resemblance between the two patterns encourages the speculation that the cold climate of the Y-D could have resulted from the slow-down of the THC which was induced by an input of freshwater, such as the discharge of the meltwater from the continental ice sheets. The pattern of the model-generated change, however, does not extend sufficiently toward low latitudes compared to the pattern of the Y-D/Alleröd difference determined from proxy data. Furthermore, the simulated cooling at Summit, Greenland, appears to be smaller than the actual cooling estimated from the isotopic analysis of ice cores (GRIP Members, 1993). These descrepancies result partly from the use of simulated modern climate as a control rather than the much colder climate of the last deglaciation period. The extensive coverage of sea ice during the cold deglaciation period could have not only extended the region of cooling towards lower latitudes but also increased its magnitude. Therefore, it is desirable to conduct additional freshwater experiments using a simulated deglacial climate as a control.

Superimposed upon the weakening and intensification of the THC which occurs over the period of several centuries, is a multidecadal fluctuation of the THC which follows the sudden onset of the freshwater discharge at the beginning of the experiment (Fig. 9a). The multidecadal fluctuation of the THC is approximately in-phase with the corresponding fluctuations of SSS and SST. Shortly after the start of the water discharge, a very rapid drop of both SSS and SST occurs, followed by large oscillations of both variables with a time-scale ranging from a few decades to a century (Figs. 9b, c). The amplitudes of the oscillations gradually decrease until the termination of freshwater discharge (i.e., the 500th year). The ampli-

Fig. 4. Streamfunction of the THC in the Atlantic Ocean of the coupled model in units of sverdrups. (a) Control experiment (100-year average taken just prior to starting the freshwater integration). (b) Average over years 401–500 of the freshwater integration. (c) Average over years 901–1000 of the freshwater integration. On the left-hand side of each panel, depth is indicated in meters (from MS97).

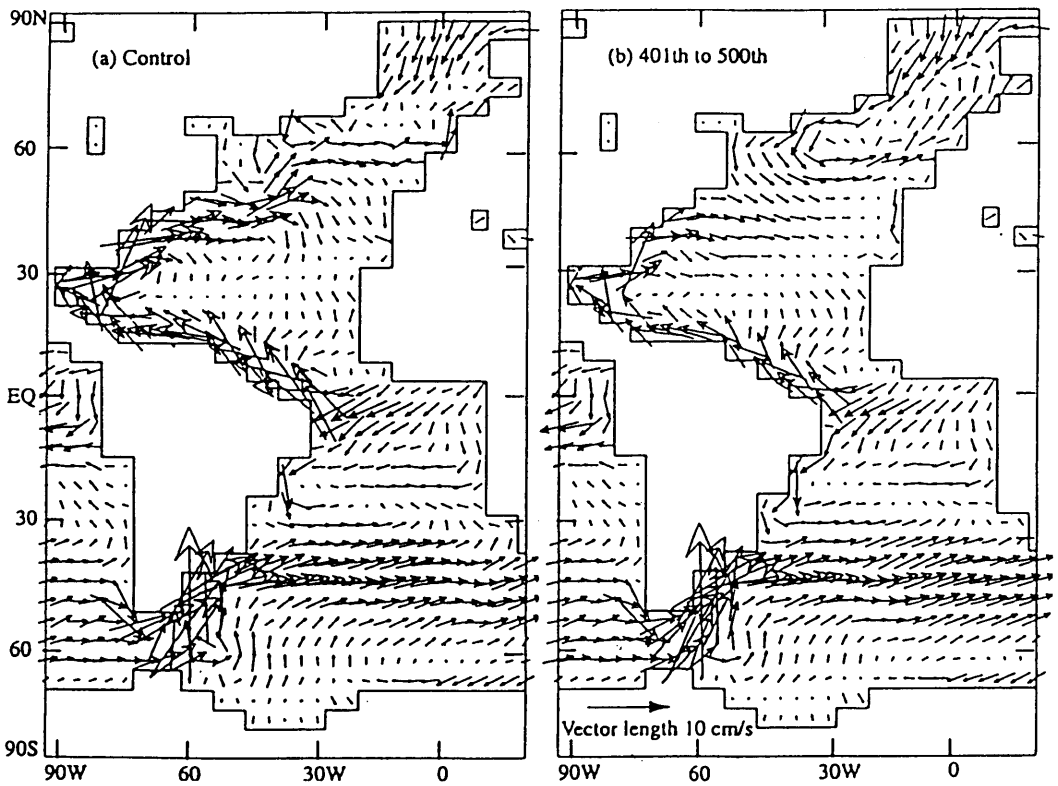

Fig. 5. Map of surface current vectors. (a) Control experiment (100-year average taken just prior to starting the freshwater integration). (b) Average over year 401–500 of the freshwater integration (from MS97).

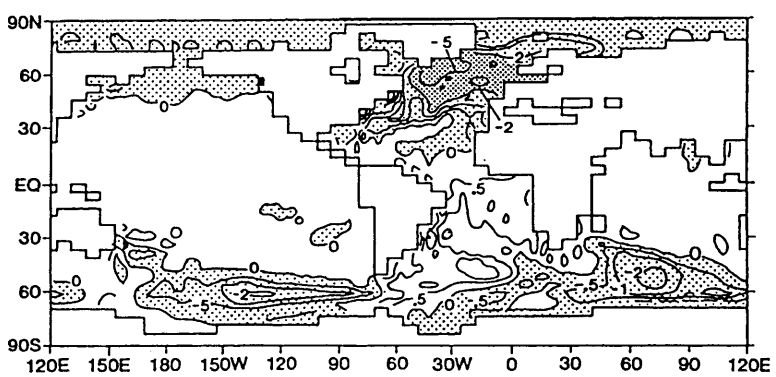

Fig. 6. Geographical distribution of SST anomalies (°C) averaged over year 401–500 of the freshwater integration. The anomalies are defined as the difference between the freshwater and the control integrations (from MS97). The logarithmic contouring is employed with contour values of 0.5, 1, 2 and 5.

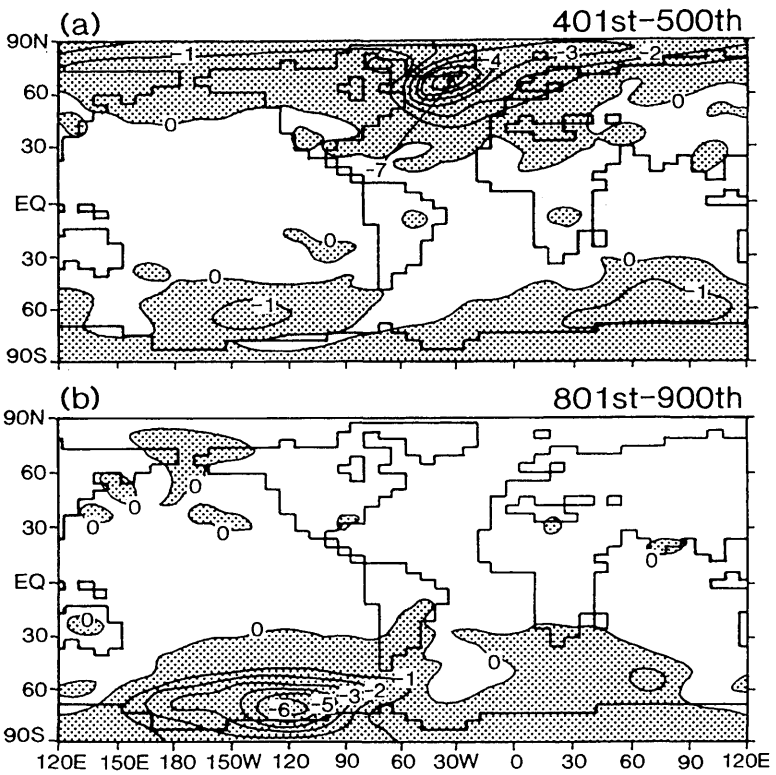

Fig. 7. The geographical distributions of surface air temperature anomalies (°C) averaged over (b) years 401–500 and (d) years 801–900 of the freshwater integration. The anomalies represent the difference between the freshwater and the control integrations (from MS97).

tude, however, increases again a few hundred years later, resulting in repeated, almost abrupt warming and cooling (Fig. 9b). The large fluctuations in surface conditions are approximately in phase with the fluctuations of the THC, as noted above.

Because of the sudden onset of the freshwater discharge, the surface of the North Atlantic Ocean is capped by low salinity water with relatively low density. The capping reduces markedly the convective cooling of water, and accordingly, the production of negative buoyancy in the sinking region of the THC. Thus, the THC weakens almost instantaneously, inducing the multidecadal oscillation which involves the multidecadal fluctuations of not only the intensity of the THC but also SSS and SST. The fluctuation in the density of near-surface water thus generated causes the corresponding variation in convective activity, which mixes the cold and fresh surface water with warmer and more saline subsurface water. The temporal variation in the intensity of convective activity (Fig. 9d), in turn, further enhances the variability of both SST and SSS.

The reduction of SST during the period of freshwater discharge and its increase after the termination of the discharge are much more gradual than the abrupt reduction and increase of surface air temperature which occurred at the beginning and end of the Younger Dryas period, respectively. However, the rapid changes of SST generated by the multidecadal fluctuation of the THC are almost as abrupt as the rise and fall of SST associated with the Y-D. In an earlier numerical experiment, Manabe and Stouffer (1995) generated even more abrupt falls and rises of SST by increasing the rate of freshwater discharge. In response to the sudden onset of a massive discharge of freshwater into the northern North Atlantic at the rate of 1 Sv, the THC weakened very rapidly, thereby lowering the SST in

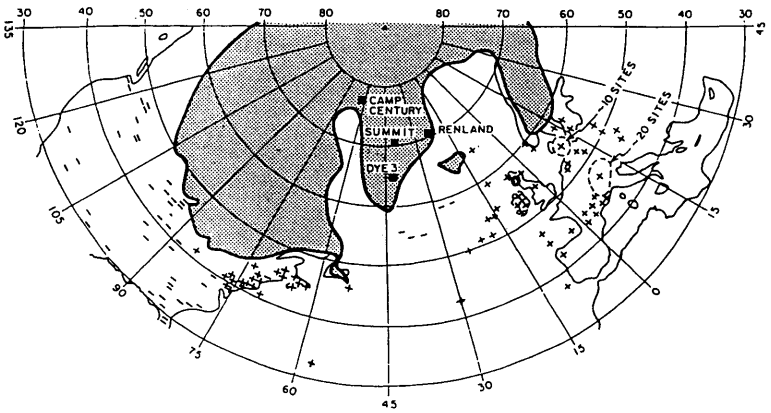

Fig. 8. Map prepared by D. Peteet showing sites of ocean sediment (planktonic forams) and bog sediments (pollen grains) where records covering the interval of deglaciation are available. The pluses (minuses) indicate that the Younger Dryas event (Y-D) cooling is seen (not seen). Two pluses are added by the present authors at 43.5°N, 29.9°W and 33.7°N, 57.6°W, referring to the studies of Keigwin and Lehman (1994), and Keigwin and Jones (1989), respectively. The locations of the Greenland ice cores (all show the Y-D) are also given. The shaded region shows the area coverage of the ice cap at the time of the Y-D (from Broecker, 1995). See also Fig. 6 of Peteet (1995) which indicates the global distribution of polynological evidence for the Y-D cooling. This figure is taken from Broecker (1995).

Denmark Strait and surrounding regions. Upon suspension of the freshwater discharge, the THC exhibited a complex transient behavior, including an almost abrupt fall, rise and fall of SST for several decades followed by a gradual recovery toward the initial state. One can speculate that, for example, multidecadal fluctuations of isotopic temperature between Bølling and Y-D, which are evident in the high-resolution records from Greenland ice cores (e.g., Fig. 2 of Grootes et al., 1993), may also be caused by the abrupt onset and termination of massive discharge of meltwater.

The time-scale of the fluctuation of the THC, induced by the freshwater discharge in the coupled model, is similar to that of the much weaker, irregular oscillation of the THC which was found by Delworth et al. (1993) in the unforced, control integration of the coupled model. The pattern of SST anomalies associated with this irregular oscillation bears an encouraging resemblance to the pattern of observed multidecadal variability in the North Atlantic Ocean (Kushnir, 1994). Delworth et al. (1997) also found that this irregular oscillation of the THC is partially coherent with the temporal variation of the East Greenland Current which induces the fluctuation of SSS in the Greenland Sea. The SSS variation in the Greenland Sea is preceded by large scale SSS changes in the Arctic Ocean, from where the SSS anomaly exits through the east Greenland current. The anomaly then propagates around the subpolar gyre into the Labrador Sea and the central North Atlantic (Fig. 10) in a manner similar to the so called great salinity anomaly event discribed by Dickson et al. (1988). The SSS variation mentioned above accompanies the in-phase variation of SST with amplitude up to 2°C in the Greenland Sea. Analysis of instrumental and proxy data from the last five centuries provides evidence for distinct multidecadal variability in the North Atlantic and Arctic Oceans (Mann et al., 1995). A promising path toward satisfactory assessment of such variability lies in the combination of well-designed model experiments with the analysis of both instrumental and proxy data.

3.4. Two stable equilibria

Manabe and Stouffer (1988) found that their coupled ocean-atmosphere model with the annually averaged insulation has at least 2 stable equilibria with active and inactive modes of the THC in the North Atlantic Ocean. The active mode resembles the current state of the THC with a sinking region in the northern North Atlantic, whereas the inactive mode is characterized by a

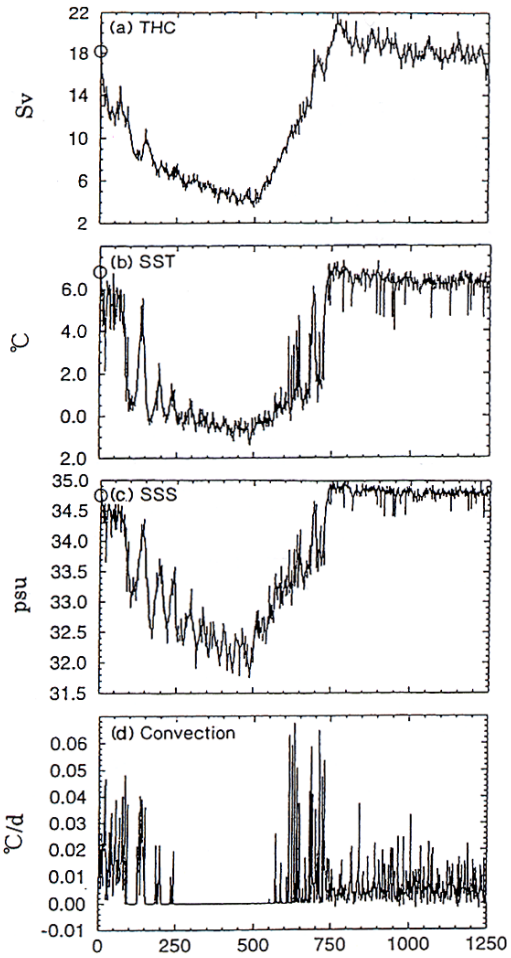

Fig. 9. Time series of annual mean values of (a) intensity of the THC (in units of Sv, i.e., 10^6 m^3 s^{-1}) defined as the maximum value of its streamfunction in the North Atlantic Ocean, (b) SST (°C), (c) SSS (psu), (d) rate of SST change (°C d^{-1}) due to convective adjustment, at a location in the Denmark Strait (30.0°W, 65.3°N) over the 1250-year period of the freshwater integration. The initial values of THC, SST, and SSS are enclosed by circles (from MS97).

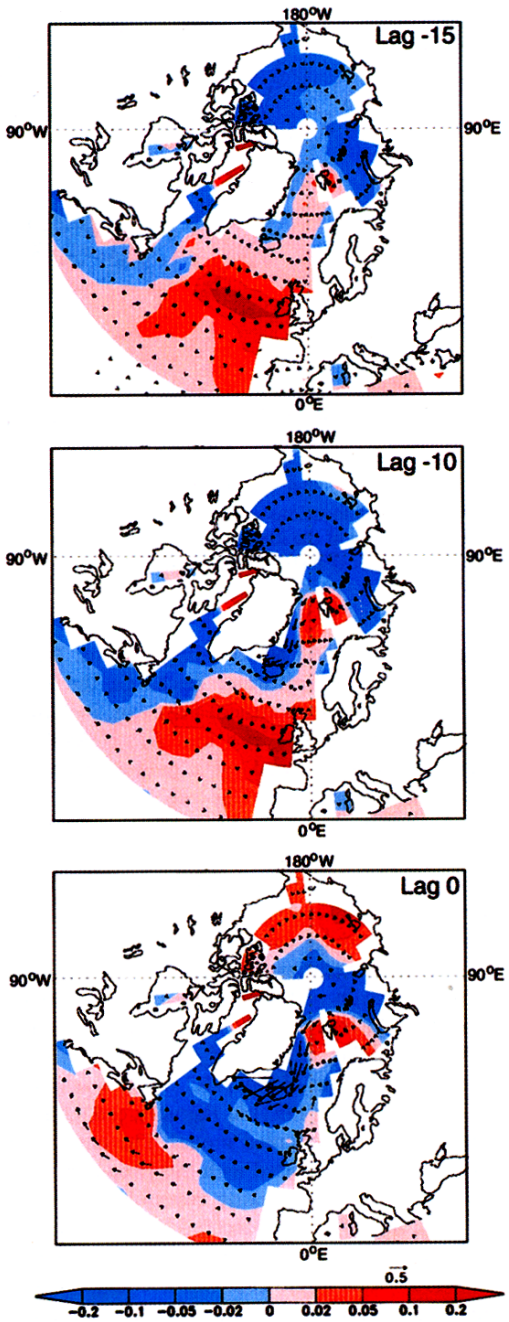

Fig. 10. Regressions of annual mean SSS at each grid point versus the time series of annual mean SST in the Denmark Strait (15°W to 26°W at 70°N). The contoured values are the slopes of the regression lines multiplied by −2 (to indicate conditions associated with an SST anomaly of −2°C). The field at Lag −15 indicates conditions 15 years prior to a −2°C SST anomaly in the Denmark Strait. Units are parts per thousand per −2°C SST anomaly. In addition, the regressions of the surface currents are indicated by the vectors. Units are cm s^{-1} per −2°C SST anomaly. For clarity of plotting, not all vectors of surface current anomalies are shown at very high latitudes (from Delworth et al., 1997).

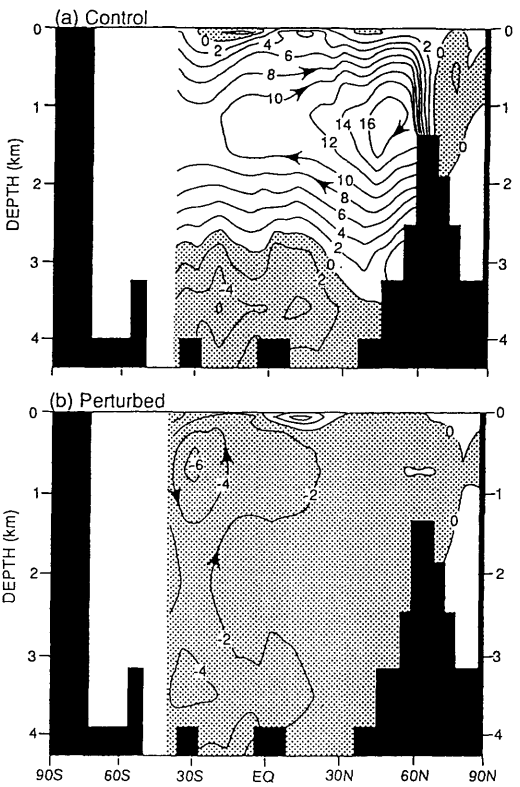

Fig. 11. The latitude-depth distributions of the stream-function of the THC (Sv) in the Atlantic Ocean obtained from the coupled model. (a) and (b) represent the stream-function of the meridional overturning of the two stable states (from Manabe and Stouffer (1999)).

weak, reverse cell of the THC with sinking motion in the circumpolar ocean of the southern hemisphere and no ventilation of subsurface water in the North Atlantic Ocean. These 2 modes appear to correspond to 2 stable modes which were obtained by Stommel (1961) using a simple box model. Manabe and Stouffer (1988) suggested further that an oceanic state similar to this inactive mode prevailed during the period of the Y-D. Paleoceanographic evidence, however, does not support this suggestion. Although the deep-sea cores from the North Atlantic Ocean indicate markedly reduced deep-water formation (Boyle and Keigwin, 1987; Keigwin and Lehman, 1994), the distribution of benthic $\delta^{13}C$ estimated by Sarnthein et al. (1994) suggests that an upper deep-water production of significant magnitude did occur during the Y-D. Paleoceanographic evidence (Boyle and Keigwin, 1987; Duplessy et al., 1988) indicates that the Atlantic Ocean of the last glacial maximum (LGM) is also significantly different from the inactive mode of the THC obtained by Manabe and Stouffer (1988). It is characterized by not only the absence of lower deep-water production and enhanced northward penetration of the Antarctic bottom water, but also significant ventilation of the upper deep-water. Thus, it is likely that the North Atlantic Ocean of the Y-D or the LGM are more similar to the transient state of a weakened and shallow THC (obtained from the present experiment) than the equilibrium state of the inactive THC obtained earlier by Manabe and Stouffer (1988).

The coupled model used here also possesses the 2 stable equilibria (Manabe and Stouffer, 1999). The distributions of the streamfunctions of the 2 modes (Fig.11) of the THC resemble what was obtained earlier with a coupled model with annual mean insulation (Manabe and Stouffer, 1988). Once it is induced, the state of the inactive mode of the reverse THC is stable and remains stable over the period of at least several thousand years. Despite the heating due to the vertical thermal diffusion, the temperature of the bottom water does not increase because of the cooling due to the formation of the Antarctic bottom water. Thus the stratification of the deeper layer of the model ocean remains unchanged, preventing the re-activation of the THC.

These results differ from what Schiller et al. (1997) obtained using a coupled ocean-atmosphere model developed at the Max-Planck-Institute (MPI) in Hamburg, Germany. In response to the input of a massive amount of freshwater, the THC of the MPI model collapsed into the inactive mode of the reverse THC, which is qualitatively similar to the inactive mode obtained by Manabe and Stouffer (1988, 1999). However, upon termination of the freshwater discharge, the THC intensified rapidly, eventually regaining its original intensity, in sharp contrast to the behavior of the inactive, reverse mode obtained by Manabe and Stouffer (1988). The difference in behavior between the GFDL and MPI models identified above may be attributable to the difference in the magnitude of diapycnal diffusion. Specifically, the oceanic component of the coupled model used by Schiller et al. (1997) employs the 1st-order, upstream finite difference

technique for the computation of advection and, therefore, has relatively large implicit, computational diffusion (Wurtele, 1961; Molencamp, 1968). It is likely that the large diapycnal diffusion of potential temperature and salinity facilitates the movement of water across isopycnal surfaces, resulting in the reintensification of the THC and the resumption of North Atlantic deep-water formation which occurred after the termination of freshwater discharge in the numerical experiment conducted by Schiller et al.

In order to evaluate this speculation, Manabe and Stouffer (1999) recently conducted a similar freshwater experiment using a modified version of the GFDL coupled model in which the coefficient of vertical subgrid scale diffusion in the upper 2 km layer of oceans is several times larger than in the standard version. Although the reverse THC was produced in this version of the coupled model in response to the massive discharge of freshwater, it began to transform rapidly back to the original, direct THC as soon as the freshwater discharge was terminated, in qualitative conformity with the behavior of the MPI model.

Our results clearly indicate that the inactive mode of the reverse THC is not a stable state in a coupled model with a large diapycnal diffusion coefficient. Measurement of the invasion of anthropogenic tracers, such as bomb tritium and ^{3}He, have indicated that the coefficient of vertical diapicnal mixing in the ocean thermocline of the subtropical North Atlantic is less than 0.1 $cm^2\ s^{-1}$ (Jenkins, 1980) or about 0.2 $cm^{-2}\ s^{-1}$ (Rooth and Östlund, 1972). Based upon the results from a recent field experiment (Ledwell et al., 1994), the most likely value of the effective vertical diffusion coefficient in the ocean thermocline is 0.1–0.2 $cm^2\ s^{-1}$. Even the standard version of the GFDL coupled model, with the stable mode of the inactive, reverse THC, has a larger vertical diffusion coefficient than these values. Therefore, it is highly likely that the mode of the reverse THC is also stable in the real Atlantic Ocean which has a small vertical diffusion coefficient.

When a coupled model with sufficiently low vertical diffusion coefficient enters the stable state of the reverse THC, it does not get out of it easily (Rahmstorf, 1995). However, the abrupt warming occurred at the end of the cold state of Y-D. This is another important reason why we believe that the cold state of Y-D was not a stable state of the reverse THC with no deep-water formation in the North Atlantic Ocean. Instead, it is a temporarily weakened state of the THC. As noted already, the paleoceanographic signature of deep-water formation is consistent with this assertion.

4. Future climate change

4.1. Global warming experiments

The thermohaline circulation could also change associated with global warming in the future. In response to the increase of atmospheric carbon dioxide, the absolute humidity as well as the temperature of the troposphere increase, enhancing the poleward transport of water vapor and causing the large increase of precipitation and runoff in high latitudes. The increased supply of freshwater in the Arctic and surrounding oceans could weaken the THC. This is what happened in the multiple-century global warming experiments conducted by Manabe and Stouffer (1993, 1994). Their study is hereafter identified as MS94. This essay discusses the results obtained from these global warming experiments.

In order to explore the future change of climate over many centuries, 3 long-term integrations of the coupled model were performed with temporal variations of atmospheric carbon dioxide, illustrated in Fig. 12a. In addition to the control integration referred here as *S*-integration, in which the atmospheric concentration of carbon dioxide is held fixed, 2 long-term integrations of the coupled model were performed. In one integration, referred to as the $4 \times C$ integration, the CO_2 concentration in the atmosphere increased at the rate of 1%/year (compounded) until it reached the $4\times$ the normal concentration at the 140th year and remains unchanged thereafter. In another integration, referred to as the $2 \times C$ integration, the CO_2 concentration was increased at the rate of 1%/year until it reached twice the normal value at the 70th year.

The study of Walker and Kasting (1992) indicates that, if we keep burning fossil fuels at a business-as-usual pace, and continue to cut tropical rainforests, the atmospheric CO_2 could quadruple above the preindustrial level during the next few centuries. Therefore, the $2 \times C$ and $4 \times C$ senarios of future CO_2 increase described above may not be excessive.

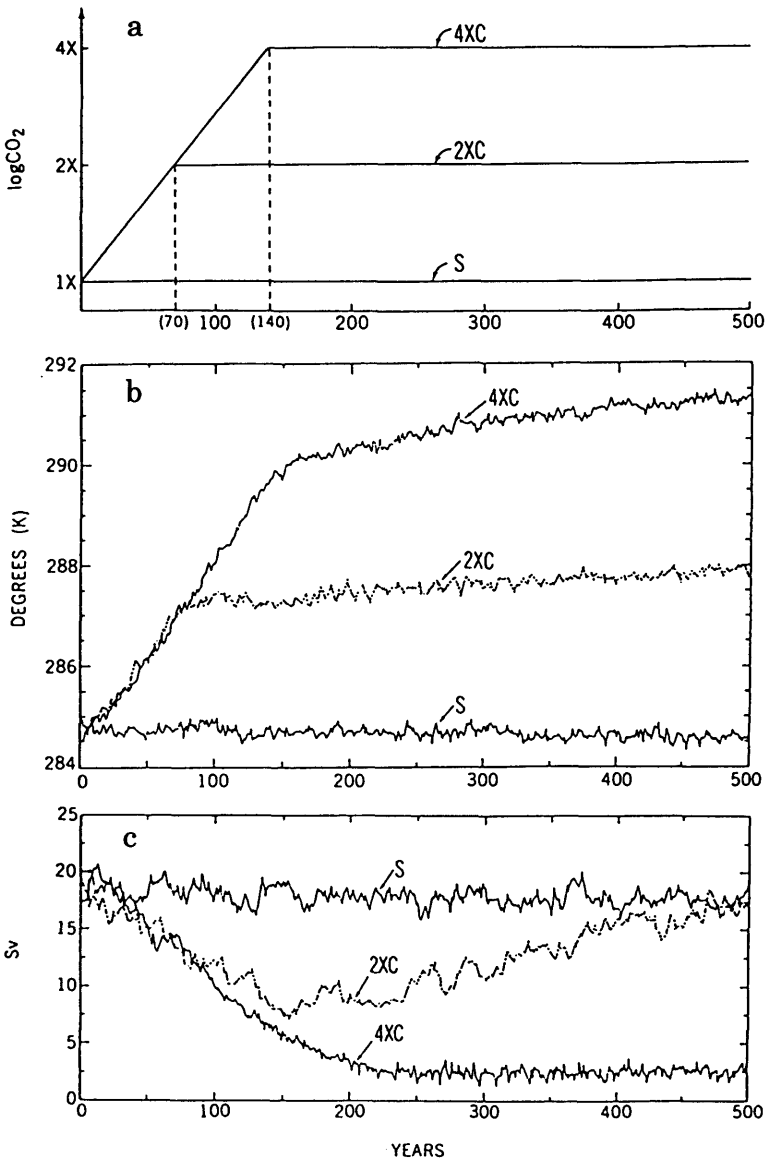

Fig. 12. Temporal variations of: (a) logarithm of atmospheric CO_2 concentration; (b) global mean surface air temperature (K); (c) the intensity of the THC in the north Atlantic; obtained from 4 × C, 2 × C and S (from MS94). Here, the intensity of the THC is defined as the maximum value (Sv) of the streamfunction representing the meridional overturning in the North Atlantic Ocean.

4.2. Model response

Fig. 12b contains the time series of global mean surface air temperature from the 4 × C, 2 × C, and *S*-integrations. During the first 140 years of the 4 × C integration, the global mean surface air temperature increases by about 5°C at the rate of ~3.5°C per century. After the 140th year, the global mean surface air temperature increases very slowly by an additional 1.5°C despite the absence

of further CO_2 increase in the model atmosphere. The large thermal inertia of the deep ocean is mainly responsible for this residual warming.

A qualitatively similar feature is evident in the time series of the 2 × C integration. During the first 70 years, the global mean temperature increases by 2.2°C, again at the rate of 3.5°C per century. After atmospheric CO_2 stops increasing at the 70th year, the global mean surface air temperature increases by an additional 1°C.

Fig. 12c indicates that, in the 4 × C, the THC nearly vanishes in the North Atlantic during the first 250 years of the integration. The near-extinction of the THC (Fig. 13) is attributable mainly to the capping of oceans by relatively fresh water in high latitudes, where the supply of water to the ocean surface increases markedly. In high northern latitudes poleward of 50°N, the supply of freshwater due to the excess of precipitation over evaporation increases by about 0.28 Sv over the 500 years period of the 4 × C experiment because of the enhanced poleward transport of water vapor in the warmer model troposphere (refer to Fig. 13 of MS94).

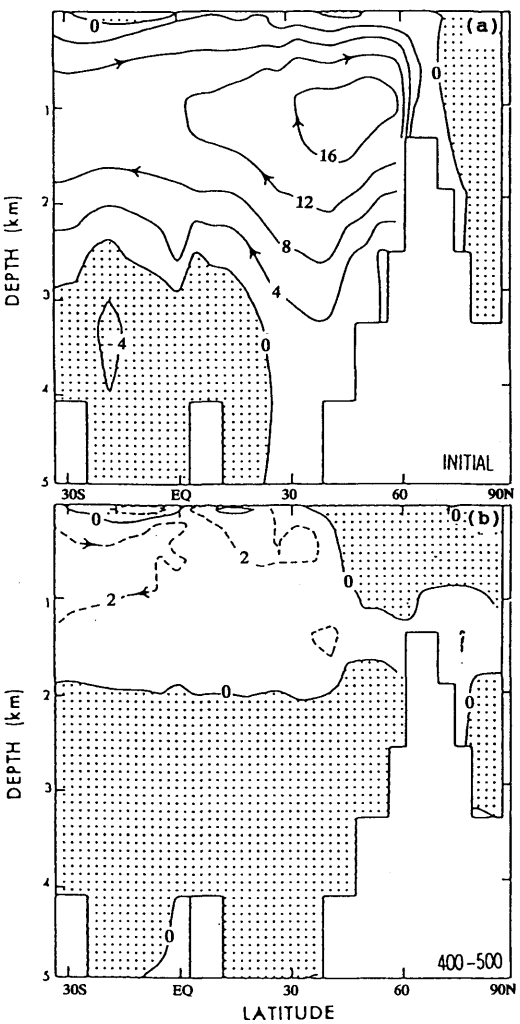

Fig. 13. Streamfunction of meridional circulation (Sv) in the Atlantic Ocean from the 4 × C. (a) Initial condition. (b) Average over the 400th–500th year (from MS94).

The evolution of the THC in 4 × C described above can be compared with the 2 × C in which the atmospheric carbon dioxide increases until it doubles. In the 2 × C, the THC in the North Atlantic again keeps weakening long after the 70th year when atmospheric CO_2 stops increasing and the rates of surface warming and freshening are abruptly reduced (Fig. 12); the THC is eventually weakens to less than half of its original intensity (Fig. 14). However, the THC begins to recover very slowly around the 150th year of the integration, resulting from the reduction in the meridional density gradient of the upper layers of the model ocean. Because of the reduction in the rate of the upward advection of cold water that accompanies the weakening of the THC, a large warming of the subsurface layer takes place in the 2 × C between the equator and 45°N latitudes, thereby increasing the meridional density gradient. Since the thermal expansion coefficient of sea water depends upon temperature, the general warming also results in the increase of meridional density gradient in the upper oceanic layer as water becomes lighter in low than high latitudes. The resulting increase in not only the meridional density gradient in the upper layer of the north Atlantic appears to be responsible for the gradual recovery of the intensity of the THC after the 150th year of the 2 × C.

The structure of the THC at its weakest stage in the 2 × C integration differs from the stable states of reverse cell which Manabe and Stouffer (1988, 1989) obtained and was discussed in Subsection 3.3. It appears that the initial weakening of the THC from the normal to the weakest is not the transition from one stable mode to another. Instead, it is similar to the temporary weakening of the THC which occurred in the

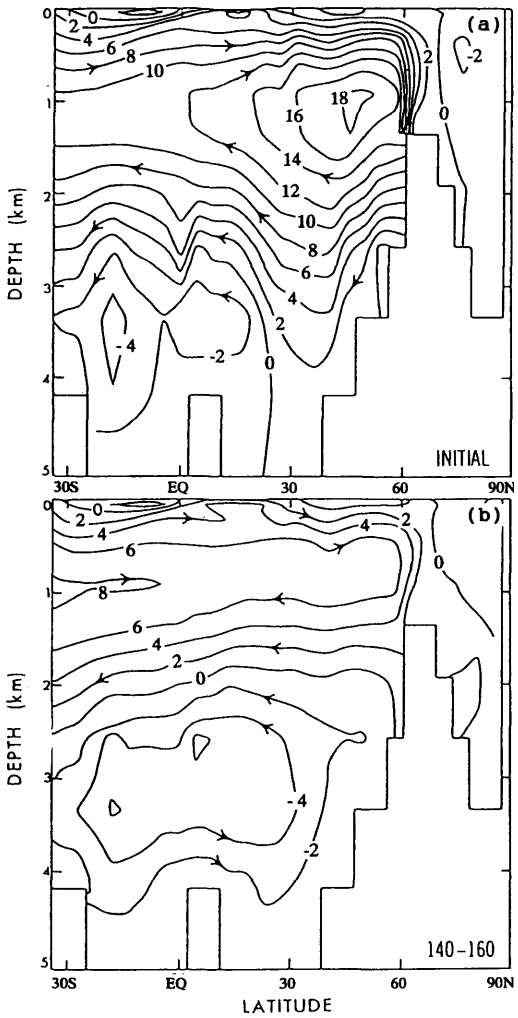

Fig. 14. Streamfunction of meridional circulation (Sv) in the Atlantic Ocean from the 2 × C. (a) Initial condition. (b) Average over the 140th–100th year (from MS94).

freshwater discharge experiment discussed in Section 3.

Recently, the 4 × C integrations of the coupled model were extended beyond the 500th year to 5000th year. Fig. 15 illustrates the time series of the 100-year mean intensity of the THC over the first 3000 years. It shows that, although the THC remains to be very weak from 250th to 900th year of the 4 × C integration, it begins to reintensify around 1000th year and fully regains the original intensity by the 1600th year. It appears that this very slow recovery of the THC is attributable to the very slow rise of the bottom water temperature that begins around the 250th year. The capping of oceanic surface by low salinity water occurs not only in high north Atlantic latitudes but also in the immediate vicinity of the Antarctic Continent, markedly reducing the rate of the bottom water formation there. Thus, the heating of the bottom water due to the downward thermal diffusion exceeds the cooling due to the Antarctic bottom water formation, thereby contributing to the gradual warming of bottom water temperature. As the temperature of the bottom water rises slowly, the static stability of deeper layers of the Atlantic Ocean is reduced, resulting in the delayed, slow recovery of the THC described above. This recovery suggests that the state of the very weak but direct THC which was reached by the 250th year of the 2 × C integration is very close to, but differs from the stable mode of the reverse cell discussed in Subsection 3.3.

Fig. 16a illustrates the geographical distribution of surface air temperature change which occurred by the 500th year of the 4 × C integration. It shows that the increase of surface air temperature is relatively small over the North Atlantic resulting from the weakening of the THC discussed above. The warming is also reduced in western Europe which is located at the downstream of the North Atlantic. In general, the increase of surface temper-

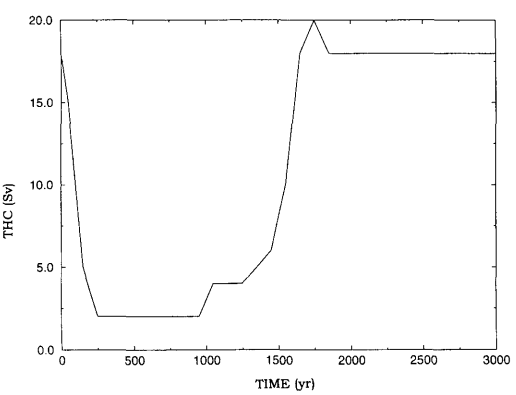

Fig. 15. Time series of the 100-year mean intensity of the THC (Sv) obtained from the 4 × C integration of the coupled model over the period of 3000 years (from MS94). Here, the intensity of the THC is defined as the maximum value of streamfunction representing the meridional overturning in the North Atlantic Ocean.

ature is much larger over continents than over oceans. The larger continental warming is attributable not only to smaller effective thermal inertia but also to smaller evaporative cooling of continental surface.

The pattern of surface air temperature change which occurs by the 500th year of the 2 × C integration is illustrated in Fig.16b. Although this pattern resembles the corresponding pattern from the 4 × C integration (Fig. 16a), this feature of reduced warming in the North Atlantic is not as pronounced. This is because the THC almost restored the original intensity by the 500th year and is no longer reducing the warming over the North Atlantic Ocean.

5. Concluding remarks

The coupled ocean-atmosphere model used here qualitatively reproduces many characteristics of climate change associated with the Y-D event and Dansgaard-Öschger oscillation. In response to the discharge of freshwater into a high-latitude belt of the North Atlantic Ocean, the THC weakens, creating the cooling pattern which resembles the pattern of the Y-D cooling, as inferred from the comprehensive analysis of ice cores and deep sea and lake sediments (Broccker, 1995). The geographical distribution of the cooling, however, is highly variable, with particularly large cooling in the northern North Atlantic and surrounding regions.

The sudden onset and termination of massive discharge of freshwater also induces the multidecadal fluctuations of the THC, SST and SSS in the coupled model. The rapid changes of SST thus generated are almost as abrupt as the rapid temperature fluctuations of the Y-D period inferred from the isotopic analysis of Greenland ice cores (Grootes et al., 1993).

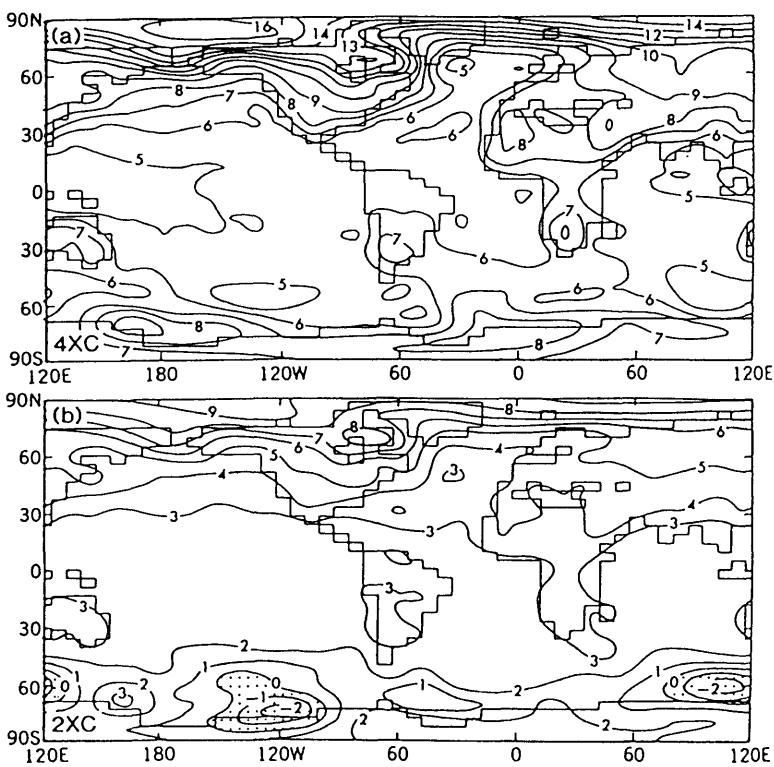

Fig. 16. Geographical distributions of the increase of annual mean surface air temperature (°C) from (a) 4 × C and (b) 2 × C (from MS94). The increase represents the difference between the 401th–500th year average of the 4 × C or 2 × C and 401th–500th year of the S.

The THC also weakens in the 2 × C (or 4 × C) integration in which the atmospheric concentrations of carbon dioxide initially increases at the rate of 1%/year until it doubles (or quadruples) and remains unchanged thereafter. The weakening, however, is not as abrupt as the initial change of the THC or its multidecadal oscillation which is induced by the sudden onset of massive freshwater discharge mentioned above. This is because the gradually increasing supply of freshwater in high latitudes, which occurs during the early stages of the 2 × C (or 4 × C) integration is not as effective in inducing the abrupt change of the THC intensity as the sudden commencement of freshwater discharge in the Y-D integration.

Recent studies of Stocker and Schmitter (1997) and Stouffer and Manabe (1998) indicate that the total weakening of the THC which occurred by the time of CO_2 doubling, for example, depends critically upon the rate of CO_2 increase. They found that the larger the rate of increase, the larger is the magnitude of reduction in the intensity of the THC that occurred by the time of the CO_2 doubling. For example, if the initial rate of CO_2 increase were significantly below 1%/year in the 4 × C integration, the magnitude of the reduction of the THC would be much smaller and the reintensification of the THC would have occurred much earlier than what happened in the 4 × C integration.

Following the path-finding study by Mitchell et al. (1995), Haywood et al. (1997) investigated the response of the coupled model to increases of not only greenhouse gases but also anthropogenic sulfate aerosols. It is assumed that the rate of future increases of the CO_2-equivalent concentration of greenhouse gases is 1%/year which may be realized in the absence of new and explicit control measures. This numerical experiment reproduces reasonably well the observed increase of global mean surface air temperature during the 20th century. They noted that the THC in this experiment starts to weaken significantly after 2010. By 2065, the intensity of the THC in the North Atlantic Ocean is reduced from 18 to 10 Sv. It is likely, however, that the magnitude and the rate of weakening could be affected not only by the temporal variation of radiative forcing but also by the model characteristics such as the formulation of subgrid scale mixing processes and the computational resolution of the oceanic component of a coupled model. For example, the coupled model used here poorly resolves the bottom topography of the North Atlantic Ocean which could critically affect the stability of the THC. It has been shown (MS94) that the rate of precipitation in high latitudes of the coupled model changes significantly when its resolution is doubled. A recent coupled model integration at MPI Hamburg, which uses higher resolution, shows that the influence of CO_2 increase on the intensity of the THC is much reduced (Private communication). In order to evaluate reliably the future change in the THC, it is therefore necessary to repeat the global warming experiments whenever a coupled model is improved substantially.

REFERENCES

Bond, G., Heinrich, H., Broecker, W., Labeyrie, L., McManus, J., Andrews, J., Huon, S., Jantschik, R., Clasen, S., Simet, C., Tedesco, K., Klas, M., Bonai, G. and Ivy, S. 1992. Evidence for massive discharges of icebergs into the North Atlantic Ocean during the last glacial period. *Nature* **360**, 245–249.

Boyle, E. A. and Keigwin, L. D. 1987. North Atlantic thermohaline circulation during the past 20,000 years linked to high-latitude surface temperature. *Nature* **330**, 35–40.

Broecker, W. S. 1995. *The glacial world according to Wally*. Eldigo Press, Lamont–Doherty Earth Observatory, Palisades, New York, 318 pp. + Appendix.

Broecker, W. S., Peteet, D. and Rind, D. 1985. Does the ocean-atmosphere system have more than one stable mode of operation? *Nature* **315**, 21–25.

Bryan, K. 1969. Climate and the ocean circulation. Part II: The ocean model. *Mon. Wea. Rev.* **97**, 806–827.

Bryan, K. and Cox, M. 1967. A numerical integration of the oceanic general circulation model. *Tellus* **19**, 54–80.

Bryan, K. and Lewis, L. 1979. A water mass model of the world ocean. *J. Geophys. Res.* **84** (C5), 2503–2517.

Delworth, T. L., Manabe, S. and Stouffer, R. J. 1993. Interdecadal variation of the thermohaline circulation in a coupled ocean-atmosphere model. *J. Climate* **6**, 1993–2011.

Delworth, T. L., Manabe, S. and Stouffer, R. J. 1997. Multidecadal variability in the Greenland Sea and surrounding regions: a coupled model simulation. *Geophys. Res. Lett.* **24**, 257–260.

Dickson, R. R., Meinke, J., Malmberg, S. A. and Lee, A. J. 1988. The "Great Salinity Anomaly" in the north-

ern North Atlantic 1968–1982. *Progress in Oceanography* **20**, 103–151.

Dixon, K. W., Bullister, J. L., Gamon, R. H. and Stouffer, R. J. 1996. Examining a coupled air-sea model using CFCs as oceanic tracers. *Geophys. Res. Lett.* **23**, 1957–1960.

Duplessy, J.-C., Shackleton, N. J., Fairbanks, R. G., Labeyrie, L., Oppo, D. and Kallel, N. 1988. Deep-water source variation during the last climate cycle and their impact on the global deep water circulation. *Paleoceanography* **3**, 343–360.

Fairbanks, R. G. 1989. A 17,000 year glacio-lustatic sea level record: Influence of glacial melting rates on the Younger Dryas event and deep-ocean circulation. *Nature* **342**, 637–642.

Gordon, C. T. and Stern, W. 1982. A description of the GFDL global spectral model. *Mon. Wea. Rev.* **110**, 625–644.

Grootes, P. M., Stulver, M., White, J. W. C., Johnsen, S. and Jouzel, J. 1993. Comparison of oxygen isotope records from the GISP2 and GRIP Greenland ice cores, *Nature* **366**, 552–554.

GRIP Members. 1993. Climate instability during the last interglacial period recorded in the GRIP ice core. *Nature* **364**, 203–207.

Haywood, J. M., Stouffer, R. J., Wetherald, R. T., Manabe, S. and Ramaswamy, V. 1997. Transient response of a coupled model to estimated changes in greenhouse gas and sulfate concentrations. *Geophys. Res. Lett.* **24**, 1335–1338.

Jenkins, W. J. 1980. Tritium and ^{3}He in the Sargasso Sea. *Marine Research* **38**, 533–569.

Keigwin, L.D. and Jones, G. A. 1989. Glacial-Holocene stratigraphy, chronology and paleoceanographic observations on some North Atlantic sediment drift. *Deep-Sea Res.* **36**, 845–867.

Keigwin, L. D. and Lehman, S. J. 1994. Deep circulation linked to Heinrich event 1 and Younger Dryas in a middepth North Atlantic core. *Paleoceanography* **9**, 185–194.

Kushnir, Y. 1994. Interdecadal variation in North Atlantic sea surface temperature and associated atmospheric conditions, *J. Climate* **7**, 141–157.

Ledwell, J. R., Watson, A. J. and Law, C. S. 1994. Evidence for slow mixing across the pycnocline from an open-ocean tracer-release experiment. *Nature* **364**, 701–703.

Manabe, S. 1969. Climate and the ocean circulation, I. The atmospheric circulation and the hydrology of the earth's surface. *Mon. Wea. Rev.* **9**, 739–774.

Manabe, S. and Bryan, K. 1969. Climate calculation with a combined ocean-atmosphere model. *J. Atmos. Sci.* **26**, 786–789.

Manabe, S. and Stouffer, R. J. 1988. Two stable equilibria of a coupled ocean-atmosphere model. *J. Climate* **1**, 841–866.

Manabe, S. and Stouffer, R. J. 1993. Century-scale effects of increased atmospheric CO_2 on the ocean-atmosphere system. *Nature* **364**, 215–218.

Manabe, S. and Stouffer, R. J. 1994. Multiple-century response of a coupled ocean-atmosphere model to an increase of atmospheric carbon dioxide. *J. Climate* **7**, 5–23.

Manabe, S. and Stouffer, R. J. 1995. Simulation of abrupt climate change induced by freshwater input to the North Atlantic Ocean. *Nature* **378**, 165–167.

Manabe, S. and Stouffer, R. J. 1997. Coupled ocean-atmosphere model response to freshwater input: comparison to Younger Dryas event. *Paleoceanography* **12**, 321–336.

Manabe, S. and Stouffer, R. J. 1999. Are two modes of thermohaline circulation stable? *Tellus* **51**, in press.

Manabe, S., Smagorinsky, J. and Strickler, R. F. 1965. Simulated climatology of a general circulation model with a hydrologic cycle. *Mon. Wea. Rev.* **93**, 769–798.

Manabe, S., Stouffer, R. J., Spelman, M. J., Bryan, K. 1991. Transient response of a coupled ocean-atmosphere model to gradual changes of atmospheric CO_2. Part I: Annual mean response. *J. Climate* **4**, 785–818.

Mann, M. E., Park, J. and Bradley, R. S. 1995. Global interdecadal and century-scale climate oscillations during the past five centuries. *Nature* **378**, 266–270.

Molencamp, C. R. 1968. Accuracy of finite difference methods applied to the advection equation. *J. Appl. Meteor.* **7**, 160–167.

Orszag, S. A. 1970. Transform method for calculating vector-coupled sums: Application to the spectral form of the vorticity equation. *J. Atmos. Sci.* **27**, 890–895.

Peteet, D. 1995. Global Younger Dryas? *Quart. Int.* **28**, 93–104.

Rahmstorf, S. 1995. Bifurcations of the Atlantic thermohaline arculation in atomosphere to changes in the hydrologic cycle. *Nature* **378**, 145–149.

Rooth, C. G. and Östlund, H. G. 1972. Penetration of tritium into the Atlantic thermocline. *Deep-Sea Res.* **19**, 481–492.

Sarnthein, M., Winn, K., Jung, S. A., Duplessy, J.-C., Labeyrie, L., Erlenkeuser, H. and Gaussen, G. 1994. Changes in east Atlantic deep water circulation over the past 30,000 years: Eight times slice reconstruction. *Paleoceanography* **9**, 209–267.

Schiller, A., Mikolajewicz, U. and Voss, R. 1997. The stability of the thermohaline circulation in a coupled ocean-atmosphere general circulation model. *Climate Dyn.* **13**, 325–348.

Stocker, T. F. and Schmitter, A. 1997. Influence of CO_2 emission rate on the stability of the thermohaline circulation. *Nature* **388**, 862–865.

Stommel, H. M. 1961. Thermohaline convection with two stable regimes of flow. *Tellus* **13**, 224–230.

Stouffer, R. J., Manabe, S., Spelman, M. J. and Bryan, K. 1989. Interhemispheric asymmetry in climate response to a gradual increase of atmospheric CO_2. *Nature* **342**, 660–662.

Stouffer, R. J. and Manabe, S. 1999. Response of a coupled ocean-atmosphere model to increasing atmo-

spheric carbon dioxide: Sensitivity to the rate of increase. *J. Climate*, in press.

Walker, J. C. G. and Kasting, J. F. 1992. Effect of fuel and forest conservation on future levels of atmospheric carbon dioxide. *Paleoceanogr. Paleoclimatol., Paleoccol.* **97**, 151–189.

Winton, M. 1997. The effect of cold climate upon North Atlantic deep water formation in a simple ocean-atmosphere model. *J. Climate* **10**, 39–51.

Wurtele, M. G. 1961. On the problem of truncation error. *Tellus* **13**, 379–391.